2023 IEEE/ASME International Conference on Advanced Intelligent Mechatronics (AIM)
June 28-30, 2023. Seattle, Washington, USA

STAR–2: A Soft Twisted-string-actuated Anthropomorphic Robotic Gripper: Design, Fabrication, and Preliminary Testing

Aaron Baker[1*], Claire Foy[1], Steven Swanbeck[2], Revanth Konda[1], and Jun Zhang[1]

***Abstract*— While numerous studies have been conducted, developing a compliant robotic gripper capable of replicating human hand grasping and manipulation capabilities is still challenging. This paper presents the design, fabrication, and preliminary testing of an anthropomorphic soft robotic gripper driven by twisted string actuators (TSAs). Termed as STAR–2, it is a second generation TSA-driven soft gripper from the Smart Robotics Laboratory at the University of Nevada, Reno. The novel design facilitated a monolithic structure comprising of a 3-degrees-of-freedom (DOF) thumb and four fingers each with 2-DOFs. On account of using tendon-based actuation and the large footprint required for the thumb, the design employed meticulously planned tendon routing within the monolithic structure. Preliminary results showed STAR–2's enhanced ability to demonstrate grasp taxonomies and dexterity over STAR–1.**

I. Introduction

Most existing high-performance robotic grippers are made of rigid structures and actuators. While rigid grippers offer high grasp strengths, dexterity, and precision in executing conventional repetitive tasks, their rigidity is often not ideal for grasping delicate objects, especially in human environments where safety is critical [1]. Grasping and manipulation using soft and compliant structures or actuation mechanisms could be a potential solution to overcome this problem [2].

Soft robotic grippers have many advantages as they are lightweight, compact, and inherently safe due to compliance. However, realizing soft dexterous grippers is challenging partly due to the inherent limitations of existing compliant actuation mechanisms, such as fabrication difficulty [1], high power requirement [3], slow actuation [4], and insufficient force generation [5]. A twisted string actuator (TSA) is a promising compliant actuator that consists of two or more strings connected to a motor at one end and a load at the other end of the strings [6]. Linear actuation is generated by twisting the strings with a motor to shorten the strings' length and linearly displace the attached load [6]. [7] presented a detailed quantitative comparison of TSAs with popular soft muscle-like actuators and found that TSAs offer an advantageous combination of high force output and high energy efficiency with low mechanical complexity and weight.

We recently developed the first generation TSA-driven soft robotic gripper [8], termed as STAR–1 in this paper. [8] demonstrated TSAs' strong potential in realizing soft dexterous grippers. STAR–1 achieved 31 out of 33 Feix grasp taxonomies [9] and a score of 6 out of 10 on the Kapandji thumb dexterity test [10]. While these numbers were less compared to past studies [11]–[14], the gripper achieved the highest grasp force in comparison to other soft grippers (up to 70 N) while weighing 565 g (lowest among the soft grippers which reported Kapandji test and Feix grasp metrics). Many state-of-the-art soft grippers are pneumatically driven and are often bulky due to their actuation mechanisms' footprint [11]. STAR–1's relatively low scores on the grasp and dexterity tests were mainly because only seven TSAs were used to actuate the gripper with a simple thumb design.

Limited work has been conducted on the development of dexterous tendon-driven soft grippers, likely due to design and fabrication challenges [8]. In pneumatically-driven fingers, additional DOF can be introduced by designing separate air chambers which can be pressurized independently [11]. Designing a high-DOF tendon-driven soft gripper is challenging since additional tendon routing needs to facilitate desired motion while not interfering with other tendons. Additionally, the necessary compactness of the tendon routing makes developing manufacturing procedures difficult.

In this paper, we present the second generation of the soft twisted-string-actuated anthropomorphic robotic gripper, termed STAR–2. Firstly, the novel design of STAR–2 which results in a dexterous monolithic structure is presented. Secondly, the fabrication procedure used to realize STAR–2 is presented. Lastly, the enhanced motions and grasping capabilities of STAR–2 over STAR–1 are demonstrated. Preliminary experimental testing confirmed STAR–2's capability to realize most motions generated by the human hand including thumb opposition, thumb abduction–adduction, flexion, and extension, which could not be obtained using STAR–1.

The main contributions of this paper are: 1) Design of STAR–2, a TSA-driven anthropomorphic monolithic soft robotic gripper; 2) Development of fabrication procedures to realize STAR–2's tendon-actuation based monolithic soft structure; 3) Preliminary testing of STAR–2 including individual finger motion test, a thumb dexterity test, and basic grasp taxonomies evaluation.

This work is supported in part by the National Science Foundation under Grant Number 1852578.

*Corresponding Author

[1]A. Baker, C. Foy, R. Konda, and J. Zhang are with Department of Mechanical Engineering at the University of Nevada, Reno, NV 89557, USA (email: {aaronfox.baker, clairefoy, rkonda}@nevada.unr.edu, jun@unr.edu)

[2]S. Swanbeck is with Department of Mechanical Engineering at The University of Texas at Austin, TX 78712, USA (email: stevenswanbeck@utexas.edu)

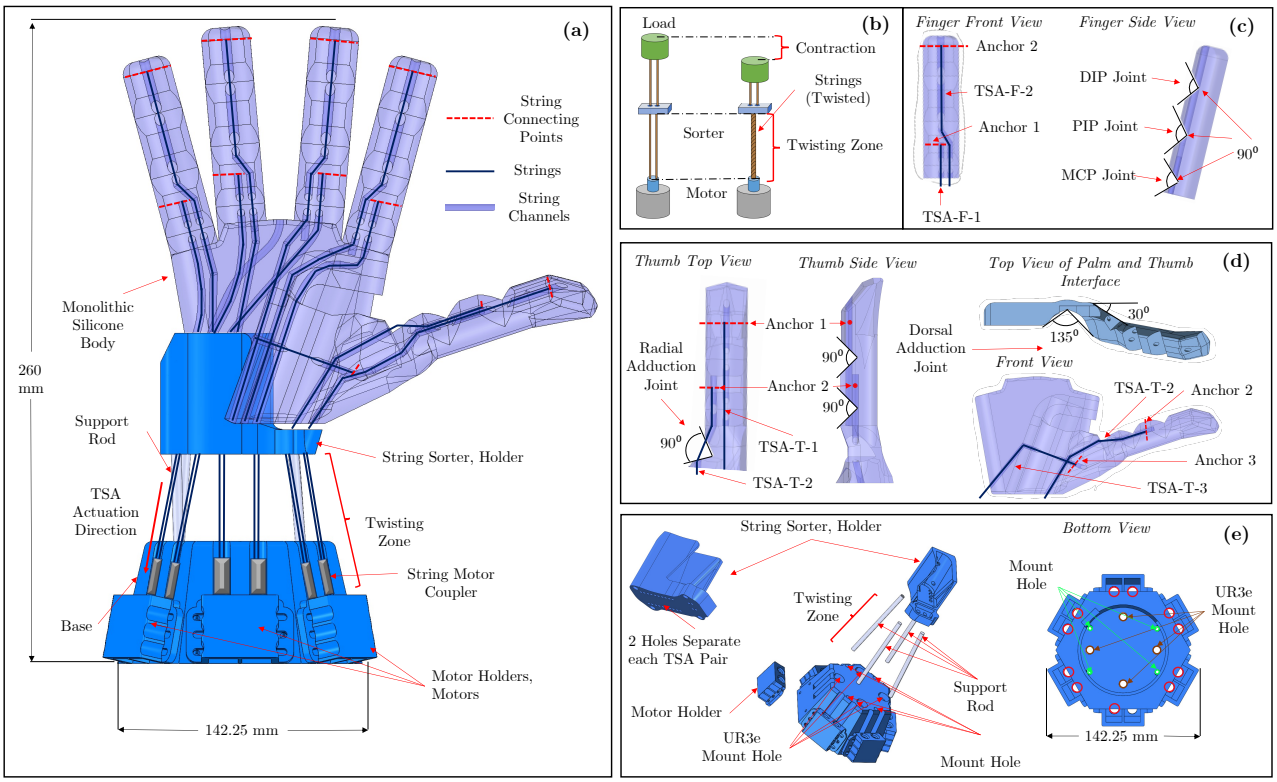

Fig. 1. Design of the different components of STAR–2. (a) Overall design of STAR–2. (b) TSA with a constant twisting zone. (c) Finger design. (d) Thumb design. (e) Base design. In the base's bottom view, the utilized motor slots are highlighted in red.

II. Design

The proposed gripper design consisted of four fingers and a thumb (Fig. 1(a)). The design utilized eleven TSAs with each finger using 2-DOFs and the thumb using 3-DOFs. With a constant twisting zone configuration the TSA strings were restricted to twisting outside the gripper's silicone body (Fig. 1(b)). The strings' twisting caused the portion of the strings inside the gripper to reduce in length (Fig. 1(b)), which generated motion. More details of the actuation mechanism can be found in Section II.C.

A. Design Considerations

1) Fingers other than thumb: Similar to STAR–1 [8], STAR–2 does show some variation with the human hand in terms of shapes, sizes, and tendon (string) placement: Unlike a human hand, all the fingers of STAR–2 were identical. Each finger consisted of three 90° "V" shaped wedges which 1) generate three finger segments analogous to the distal, middle, and proximal phalanges of a human finger, 2) act as pseudo-joints analogous to the metacarpophalangeal (MCP), proximal interphalangeal (PIP), and distal interphalangeal (DIP) joints of a human finger (Fig. 1(c)).

A key enhancement of STAR–2 finger design over STAR–1 [8] was the mode of actuation. Similar to the flexor digitorum profundus (FDP) and flexor digitorum superficialis (FDS) tendons which support the inward bending of human fingers from their respective DIP and PIP joints, each finger of STAR–2 consisted of two DOFs: One TSA (TSA-F-1) was responsible for actuating the wedge corresponding to the MCP joint, and the other TSA (TSA-F-2) was responsible for actuation of all the wedges simultaneously (Fig. 1(c)). TSA actuation resulted in two modes of finger flexion. Similar actuation has been demonstrated for pneumatically driven soft fingers [11]. The silicone elastomer's elastic nature was leveraged for finger extension. More details on the tendon routing are presented in Section II.B.(1).

2) Thumb: STAR–1's thumb was a monolithic structure attached to the gripper using silicone rubber adhesive (SIL-Poxy, Smooth-On) [8]. The thumb had 2-DOF for flexion and dorsal adduction ("roll" actuation in [8]) and had three joints resulting in three segments. This resulted in the thumb's higher reach toward other fingers. Despite these efforts, the previous thumb design generated a 6 out of 10 score on the Kapandji test. The thumb was unable to reach multiple points on the little finger, which demanded a larger range of thumb motion [8] and partly motivated this current study.

The following changes were made to STAR–2's thumb design: Firstly, along with dorsal adduction, radial adduction is also largely responsible for grasping and manipulation [15]. Therefore, an additional DOF was designed to facil-

itate the thumb's radial adduction, besides the existing two DOFs responsible for flexion and dorsal adduction motions. Secondly, for thumb opposition, the thumb pad was arranged antipodally facing the middle finger's distal pad in its rest position. The thumb assembly was placed at a 30° outward angle from the palm and fingers' plane (Fig. 1(d)). A wedge cut diagonally across the palm acted as a pseudo joint and facilitated thumb dorsal abduction–adduction motion. For achieving radial and dorsal abduction, silicone elastomer's elastic nature was leveraged. Thirdly, the thumb design consisted of two segments joined by two "V" shaped wedges (Fig. 1(d)) for enhanced biomimicry. Lastly, inspired from the thumb's distal phalanx bone [16], the thumb's tip had a rounded end with an ellipsoid structure (Fig. 1(d)), to improve thumb's grasping.

B. Tendon Routing and Placement

To avoid the embedded strings' contact with the silicone, all the tendon routing channels consisted of polytetrafluoroethylene (PTFE) tubes for housing the TSA strings.

1) Fingers other than thumb: A critical challenge to realize 2-DOF finger motion through tendon-based actuation was the tendon placement and their respective connecting points to the fingers. In pneumatically-driven fingers, a second DOF could be added by dividing the finger into two segments with separate air chambers which can be pressurized independently [11]. Such increment is difficult in tendon-driven fingers. STAR–2's fingers utilize both tendons in the frontal configuration for actuation (Fig. 1(c)). As a result, the stiffness tuning capability from STAR–1 [8] was traded off for enhanced actuation capabilities. This was done because STAR–1's stiffness tuning capabilities had relatively mild effect on the performance [8].

Each finger consisted of two connecting points: 1) Anchor 1 – at the end of the finger's first segment closest to the palm, 2) Anchor 2 – at the finger tip (Fig. 1(c)). The first channel accommodating TSA-F-1 started from the finger's base and ended at Anchor 1. This channel coincided with the central axis with respect to the finger's inner face and was offset towards the finger's inner face with respect to finger's central axis. The second channel accommodating TSA-F-2, started from the base and remained parallel to the first route until the first route ended (Fig. 1(c)). Then the second channel inclined towards the central axis with respect to the finger's inner face until it intersected with the central axis. After this point, the second channel remained in–line with the first channel. Due to the second channel's initial offset relative to the first channel, actuating TSA-F-2 resulted in a mild sideward motion depending on the location of the second channel relative to the first channel. In anticipation of this motion, the channels were arranged for the index and middle fingers versus the ring and little fingers to be symmetrical about the center line of the palm. For index and middle fingers, the second channel was on the first channel's left; For ring and little fingers, the second channel was on the first channel's right (Fig. 1(a)). This generated a clenched fist motion when all four TSA-F-2 actuators were activated.

2) Thumb: The thumb flexion was realized using TSA-T-1 (Fig. 1(d)). For thumb flexion, the string attachment point, labeled as Anchor 1, was located at the thumb's tip. From Anchor 1, the strings contorted downwards along a channel which was parallel to thumb's inner face. The thumb radial adduction [15] was realized using TSA-T-2. For thumb radial adduction, the string attachment point, labeled as Anchor 2, was located on the inner surface between the thumb and the index finger, at the end of the first thumb segment. From Anchor 2, the strings contorted downwards along a channel which was parallel to the palm pseudo-joint's inner surface below the thumb arrangement.

The thumb dorsal adduction [15] was realized using TSA-T-3. For dorsal abduction–adduction actuation, strings were embedded in a channel which started at a connecting point, labeled as Anchor 3, on the pseudo-joint's inner face below the thumb. This channel started perpendicular to the inner face on the palm pseudo-joint and moved into the palm's left side. Then, the channel bent 90° downwards towards the gripper base. It is noted that while Fig. 1(d) shows the channel's sharp turn, this is a simplification used in the modeling process and in reality the tube was curved when placed in the mold. This mechanism leverages the low friction coefficient between PTFE pipes and string material (0.04–0.06) [17]. Our previous study showed that friction did not significantly influence the actuation [8]. With this design strategy, the whole thumb assembly is moved diagonally along the palm. By actuating the TSA-T-1 and TSA-T-2, thumb opposition can be realized. By actuating the TSA-T-2 and TSA-T-3, palmar thumb adduction can be realized.

3) Palm: While the proposed thumb design enhanced its biomimicry, it also inevitably restricted the space for the tendons routed through the palm. As a result, the palm exhibited a tightly packed tendon channel routing. The PTFE tubing thickness was reduced from 4 mm in STAR–1 to 3 mm in STAR–2. The string diameter was reduced to allow smooth string motion through the smaller tubes. To maintain a similar palm thickness as STAR–1, the tendon channels in the palm were separated into three layers with 2 mm of clearance between each adjacent layers, the palm surface, and between the palm outer surface. In each layer, each tube was at least 2 mm from the nearest tube. To reduce friction, tendon routing with sharp corners were avoided. These steps resulted in a tightly packed routing network with enough space between the tubes to allow air bubbles to escape in the casting process.

C. Base

The base (Fig. 1(e)) consisted of a holder piece that held STAR–2 in position, a sorter mechanism integrated into the holder that constrained the twisting of the strings, and a collar to hold the TSA motors. The sorter mechanism worked by threading the two strings of each TSA through separate

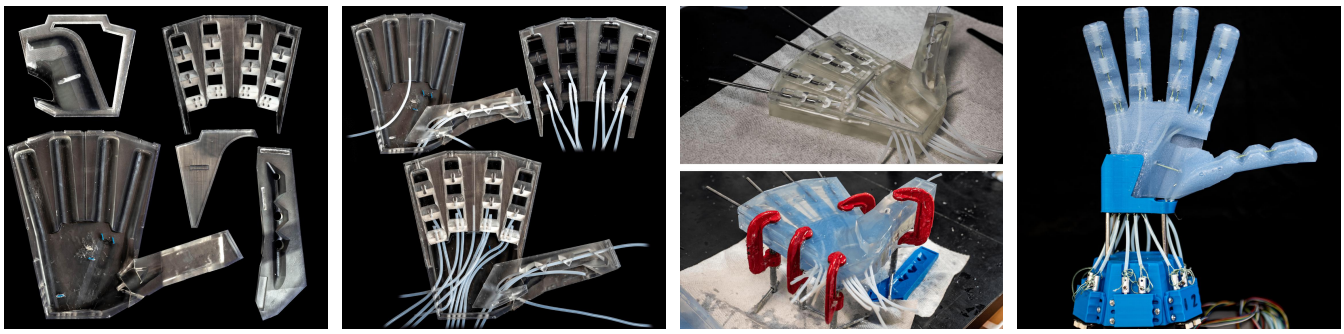

(a) (b) (c) (d)

Fig. 2. (a) First stage of fabrication: 3D printing of the mold parts. Shown: mold base, finger mid-layer, thumb lid, palm surface piece, and palm lid. (b) Second stage of fabrication: Tendon routing for the fingers and thumb actuation. From top left, clock-wise: first layer of routing, second layer of routing, combined first and second layer. (c) Third stage of fabrication: Casting the gripper using full mold assembly, silicone, and clamps. Top: fully assembled mold. Bottom: mold after the casting process. (d) Final stage of the fabrication: Clean-up of the hand, assembly of the gripper with the base.

channels in the mechanism, creating a constant twisting zone between the motors and sorter mechanism (Fig. 1(b)). This prevented string twisting within the silicone, following past studies [18]. Otherwise, directly twisting strings in channels could result in complex frictional effects due to contact with the silicon [17]. Steel rods held the collar away from the sorter, creating a twisting region large enough to provide sufficient actuation. The motor collar was hexagonal in shape with each side capable of accommodating two motors. The bottom face of the collar was designed to be compatible with a Universal Robots™ UR3e robotic manipulator (Fig. 1(e)). Overall, the gripper had a footprint of 142.25 mm × 142.25 mm and a total length of 260 mm.

III. Fabrication

A. Materials

The gripper was made of Dragon Skin™ 20 silicone two-part epoxy, which had a good balance between stiffness and compliance following STAR–1 [8]. The tendons were 0.45-mm-diameter ultra-high-molecular-weight polyethylene (UHMWPE) strings. All the channels in the gripper were equipped with PTFE tubes. PTFE tubes were selected because of their low frictional coefficient with UHMWPE strings [17]. Paper clips were used as anchor points for the strings due to their low cost. Polylactic acid (PLA) plastic was used for 3D-printing the base due to it not needing high manufacturing tolerance, with FormLabs™ Clear Resin used for 3D printing the higher tolerance mold assembly.

B. Casting Procedure

The mold's assembly process becomes complex because: 1) the PTFE tubes used in the gripper demanded to be embedded during the casting process. While STAR–1 used steel rods to form cavities for placing tubing in after casting [8], the tubing's non-constant radius of curvature in STAR–2 meant this method was not viable. In contrast, guide holes and supports in STAR–2's mold held each tube's shape and prevented collision between tubes as the silicone epoxy cured. 2) the thumb's geometry was complex compared to STAR–1. The proposed design required multiple mold parts to ensure the thumb can be removed from the mold intact with the rest of the gripper.

Designed in SolidWorks™ and then 3D printed, the mold consisted of nine parts assembled in three different stages. Fig. 2(a) shows the partly assembled mold. 6 mm diameter steel rods were set to create the straight profiled cavities of the fingers in a similar method to STAR–1 that required less effort than embedding them. This occurred after the mold was assembled and the embedded PTFE tubes' routing was realized (Fig. 2(b)–(c)). Mold release spray was used to prevent adhesion to the mold after the silicone cured.

The two-part silicone epoxy was mixed and poured into the opening of the palm surface piece, the finger mid-plane piece, and the thumb mid-plane piece of the assembled mold. As air bubbles could cause performance compromising discontinuities in the gripper, care was taken to remove them such as tilting the mold and waiting a minute between pours. Once the mold was filled with silicone, the palm and thumb lids were secured with C-clamps to push excess silicone and air out of the mold through vents on the thumb lid and finger mid-plane piece (Fig. 2(c)). Excess silicone was poured into the thumb vent holes to fill any air cavities left. These steps minimized the amount of air bubbles trapped in the gripper.

C. Post-Casting Procedure

After the gripper extraction from the mold, silicone tabs and excess PTFE tubing were trimmed while the anchor points were constructed. For each anchor point a hole was drilled into the silicone and tubing to fit a paper clip. String was pulled through the sorter and hand, then looped around the corresponding paper clip. The sorter block held the gripper in place, routed the strings out of the gripper, and separated each string pair to prevent twisting inside the gripper. PTFE tubing was placed in the sorter block's tunnels to minimize friction caused by large curvature in the tunnel routing. Each tunnel ended with two holes to separate each

strand of a string pair. After running the strings through the sorter block, one-step silicon epoxy was applied to adhere the gripper to the sorter block. Steel rods were placed between four mounting points on bottom part of the base and sorter block, and fixed with super glue. Motors were attached to the base's sides with motor holders. The strings were ran through PTFE tubing and securely attached to their respective motor shafts through metal caps.

D. Electronics and Control

Brushed DC motors (Micro Metal Gearmotor HPCB 6V, Pololu) with 30:1 reduction gearboxes were used in the TSAs. Each motor weighed 9.5 g. A magnetic Hall-effect encoder disc (Magnetic Encoder, 12CPR, Pololu) was attached to each motor to count the motor rotations for control. This gearbox and encoder combination enabled 360 (30×12) counts per rotation, resulting in a 1° (2.78×10^{-3} rotations) sensing resolution. STAR–2 weighed 499.3g, including the actuators' weight, a significant decrease from STAR–1's weight (565g), which itself had the least weight compared to soft grippers which reported Kapandji thumb dexterity and Feix Grasp Taxonomy metrics identified in our previous study [8]. STAR–2's lower weight was due to its monolithic structure which utilized lower silicone volume compared to STAR–1. The remaining electronics were housed outside of the robot and were wired to the motors. Each motor was controlled using a brushed DC motor driver (MAX14870, Pololu). A 32-bit ARM core microcontroller (Due, Arduino) was used for motor control. For the grasping tests presented in Section IV, push-buttons were utilized for individual TSAs. A software-based proportional controller which ran on the Arduino was used to reach target values of motor turns, similar to STAR–1 [8].

IV. Preliminary Results

A. Actuation

Firstly, since all the fingers except the thumb were identical, without loss of generality, the little finger's actuation is presented. Fig. 3(a) shows the MCP joint actuation when TSA-F-1 is fully actuated, which resulted in a deflection of approximately 75° of the finger tip with respect to its initial position. Fig. 3(b) shows the actuation of the MCP, PIP, and DIP joints when TSA-F-2 is fully actuated, which resulted in a deflection of 220° of the finger tip with respect to its initial position. Secondly, the different actuation modes of the thumb are tested. Fig. 3(c) shows the thumb flexion when TSA-T-1 is fully actuated, which resulted in a deflection of approximately 180° of the thumb tip with respect to its initial position. Fig. 3(d) shows the thumb radial adduction when TSA-T-2 is fully actuated, which resulted in a deflection of 90° of the thumb tip with respect to its initial position. Fig. 3(e) shows the thumb dorsal adduction when TSA-T-3 is fully actuated, which resulted in a deflection of 135° of the thumb tip with respect to its initial position.

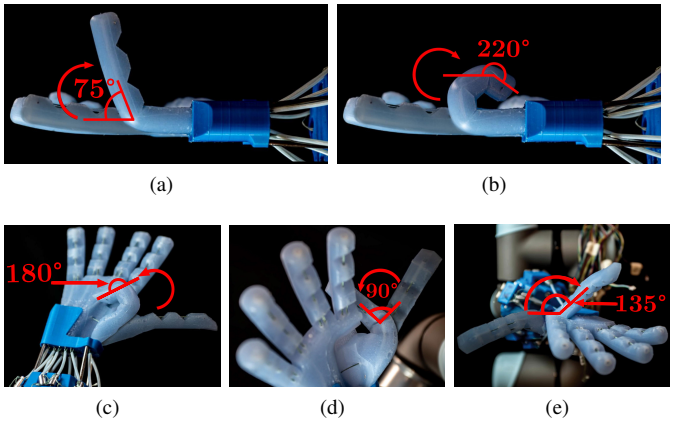

Fig. 3. The position of the finger in unactuated state (semi-opaque) and when only (a) TSA-F-1, and (b) TSA-F-2 is fully actuated, respectively. The thumb in unactuated state (semi-opaque) and when only (c) TSA-T-1, (d) TSA-T-2, and (e) TSA-T-3 is fully actuated, respectively.

B. Thumb Dexterity Test

A preliminary Kapandji test evaluation was performed to demonstrate the improvement of STAR–2's thumb over STAR–1. STAR–1 was unable to reach the four points marked in Fig. 4(a). These points were of interest when designing STAR–2, that acted as a mark of improvement over STAR–1. Through the thumb dorsal adduction actuation and flexion actuation of the thumb and little finger, STAR–2 was able to reach all the points (Fig. 4(b)–(e)).

C. Grasping Evaluation

Firstly, the parallel and adduction grip grasps are demonstrated. These were the two grasp taxonomies which STAR–1 failed to achieve [8]. The parallel grasp utilized TSA-F-1 of each finger, TSA-T-1, TSA-T-3 for thumb opposition, and TSA-T-2 for radial adduction to apply pressure on the object. The adduction grip grasp utilized the sideward motions of the middle and ring fingers upon actuating their TSA-F-2. The resulting grasps can be seen in Fig. 5(a)–(b). Secondly, three fundamental grasp taxonomies namely power, precision, and lateral grasps [19] are demonstrated. The power grasp utilized TSA-F-2 actuation of each finger and the thumb opposition actuation. For the power grasp, a cylinder and a baseball were used as shown in Fig. 5(c)–(d). The precision grasp utilized TSA-F-1 actuation of the index and middle fingers, with TSA-F-2 actuation for support. In addition, the thumb opposition TSA was also actuated. For the precision grasp a small toy was used, as shown in Fig. 5(e). The lateral grasp utilized TSA-F-1 actuation of the index finger and the thumb radial adduction TSA. For the lateral grasp, a key was used, as shown in Fig. 5(f). While this testing was not comprehensive, the obtained results demonstrated the strong potential of STAR–2's dexterity.

(a) (b) (c) (d) (e)

Fig. 4. (a) Locations which the thumb needs to touch as a part of the preliminary Kapandji test. (b)–(e) Results of the preliminary Kapandji test.

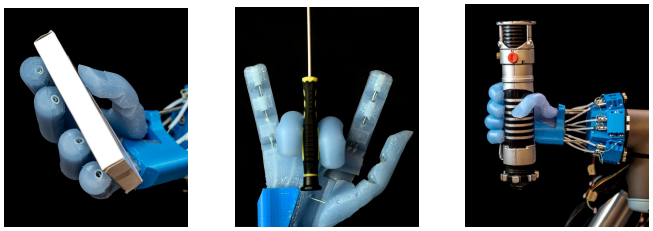

(a) (b) (c)

(d) (e) (f)

Fig. 5. (a) Parallel grasp using a small box. (b) Adduction grip using a screwdriver. Power grasp using (c) a cylinder and (d) a baseball. (e) Precision grasp using a small toy. (f) Lateral grasp using a key.

V. Conclusions and Future Work

In this paper, the second generation gripper of soft twisted-string-actuated anthropomorphic robotic gripper, STAR-2, is presented. Firstly, the design of STAR–2 was discussed. Secondly, the fabrication procedure utilized to realize the monolithic structure was described. Finally, the preliminary results which indicated STAR–2's high potential to perform dexterous manipulation, were presented. As a part of future work, firstly, STAR–2's force generation capacity will be evaluated. Secondly, STAR–2's in-hand manipulation capabilities will be studied.

References

[1] B. Shih, D. Drotman, C. Christianson, Z. Huo, R. White, H. I. Christensen, and M. T. Tolley, "Custom soft robotic gripper sensor skins for haptic object visualization," in *2017 IEEE/RSJ International Conference on Intelligent Robots and Systems (IROS)*, 2017, pp. 494–501.

[2] J. Shintake, V. Cacucciolo, D. Floreano, and H. Shea, "Soft robotic grippers," *Advanced Materials*, vol. 30, no. 29, p. 1707035, 2018.

[3] Z. Ye, Z. Chen, R. Asmatulu, and H. Chan, "Robust control of dielectric elastomer diaphragm actuator for human pulse signal tracking," *Smart Mater. Struct.*, vol. 26, no. 8, p. 085043, 2017.

[4] M. C. Yip and G. Niemeyer, "On the control and properties of supercoiled polymer artificial muscles," *IEEE Transactions on Robotics*, vol. 33, no. 3, pp. 689–699, 2017.

[5] X. Tang, K. Li, Y. Liu, D. Zhou, and J. Zhao, "A general soft robot module driven by twisted and coiled actuators," *Smart Materials and Structures*, vol. 28, no. 3, p. 035019, 2019.

[6] I. Gaponov, D. Popov, and J. H. Ryu, "Twisted string actuation systems: A study of the mathematical model and a comparison of twisted strings," *IEEE/ASME Transactions on Mechatronics*, vol. 19, no. 4, pp. 1331–1342, 2014.

[7] J. Zhang, J. Sheng, C. O'Neill, C. J. Walsh, R. J. Wood, J. H. Ryu, J. P. Desai, and M. C. Yip, "Robotic artificial muscles: Current progress and future perspectives for biomimetic actuators," *IEEE Transactions on Robotics*, vol. 35, no. 3, pp. 761–781, 2019.

[8] R. Konda, D. Bombara, S. Swanbeck, and J. Zhang, "Anthropomorphic twisted string-actuated soft robotic gripper with tendon-based stiffening," *IEEE Transactions on Robotics*, vol. 39, no. 2, pp. 1178–1195, 2023.

[9] T. Feix, J. Romero, H.-B. Schmiedmayer, A. M. Dollar, and D. Kragic, "The GRASP taxonomy of human grasp types," *IEEE Transactions on Human-Machine Systems*, vol. 46, no. 1, pp. 66–77, 2016.

[10] A. Kapandji, "Clinical test of apposition and counter-apposition of the thumb," *Annales de Chirurgie de la Main*, vol. 5, no. 1, pp. 67–73, 1986.

[11] S. Puhlmann, J. Harris, and O. Brock, "RBO Hand 3 – a platform for soft dexterous manipulation," *IEEE Transactions on Robotics*, vol. 38, no. 6, pp. 3434–3449, 2022.

[12] R. Deimel and O. Brock, "A novel type of compliant and underactuated robotic hand for dexterous grasping," *The International Journal of Robotics Research*, vol. 35, no. 1-3, pp. 161–185, 2016.

[13] J. Zhou, J. Yi, X. Chen, Z. Liu, and Z. Wang, "BCL-13: A 13-DOF soft robotic hand for dexterous grasping and in-hand manipulation," *IEEE Robotics and Automation Letters*, vol. 3, no. 4, pp. 3379–3386, 2018.

[14] J. Zhou, X. Chen, U. Chang, J.-T. Lu, C. C. Y. Leung, Y. Chen, Y. Hu, and Z. Wang, "A soft-robotic approach to anthropomorphic robotic hand dexterity," *IEEE Access*, vol. 7, pp. 101 483–101 495, 2019.

[15] V. Spartacus, "Trapeziometacarpal joint: A mechanical explanation of total prosthesis failures," in *Biomechanics*, H. Mohammadi, Ed. Rijeka: IntechOpen, 2018, ch. 6.

[16] V. K. Nanayakkara, G. Cotugno, N. Vitzilaios, D. Venetsanos, T. Nanayakkara, and M. N. Sahinkaya, "The role of morphology of the thumb in anthropomorphic grasping: A review," *Frontiers in Mechanical Engineering*, vol. 3, 2017.

[17] D. Lee, I. Gaponov, and J.-H. Ryu, "Effect of vibration on twisted string actuation through conduit at high bending angles," in *2019 IEEE/RSJ International Conference on Intelligent Robots and Systems (IROS)*. IEEE, 2019, pp. 5965–5970.

[18] B. Suthar, M. Usman, H. Seong, I. Gaponov, and J. Ryu, "Preliminary study of twisted string actuation through a conduit toward soft and wearable actuation," in *2018 IEEE International Conference on Robotics and Automation (ICRA)*, 2018, pp. 2260–2265.

[19] H. Zhou, A. Mohammadi, D. Oetomo, and G. Alici, "A novel monolithic soft robotic thumb for an anthropomorphic prosthetic hand," *IEEE Robotics and Automation Letters*, vol. 4, no. 2, pp. 602–609, 2019.